A&A 423, 155–167 (2004)
DOI: 10.1051/0004-6361:20034147

Astronomy & Astrophysics

The nature of the Galactic Center source IRS 13 revealed by high spatial resolution in the infrared⋆,⋆⋆

J. P. Maillard[1], T. Paumard[1], S. R. Stolovy[2], and F. Rigaut[3]

[1] Institut d'Astrophysique de Paris (CNRS), 98bis Bd Arago, 75014 Paris, France
e-mail: maillard@iap.fr
[2] Spitzer Science Center, CalTech, MS 220-6, Pasadena, CA 91125, USA
[3] Gemini North Headquarter, Hilo, HI 96720, USA

Received 1 August 2003 / Accepted 8 April 2004

Abstract. High spatial resolution observations in the 1 to 3.5 μm region of the Galactic Center source known historically as IRS 13 are presented. They include ground-based adaptive optics images in the H, Kp (2.12/0.4 μm) and L bands, HST-NICMOS data in filters between 1.1 and 2.2 μm, and integral field spectroscopic data from BEAR, an Imaging FTS, in the He I 2.06 μm and the Brγ line regions. Analysis of all these data provides a completely new picture of the main component, IRS 13E, which appears as a cluster of seven individual stars within a projected diameter of ~0.5″ (0.02 pc). The brightest sources, 13E1, 13E2, 13E3 which is detected as a binary, and 13E4, are all massive stars of different type. The star 13E1 is a luminous, blue object, with no detected emission line. 13E2 and 13E4 are two hot, high-mass emission line stars, 13E2 being at the WR stage and 13E4 a massive O-type star. In contrast, 13E3A and B are extremely red objects, proposed as other examples of dusty WR stars, like IRS 21 (Tanner et al. 2002). All these sources have a common westward proper motion (Ott et al. 2003) indicating they are bounded. Two other sources, detected after deconvolution of the AO images in the H and Kp bands, are also identified. One, that we call 13E5, is a red source similar to 13E3A and B, while the other one, 13E6, is probably a main sequence O star in front of the cluster. Considering this exceptional concentration of comoving massive hot stars, IRS 13E is proposed as the remaining core of a massive star cluster, which could harbor an intermediate-mass black hole (IMBH) (Portegies Zwart & McMillan 2002) of ~1300 $M_\odot$. This detection plays in favor of a scenario, first suggested by Gerhard (2001), in which the helium stars and the other hot stars in the central parsec originate from the stripping of a massive cluster formed several tens of pc from the center. This cluster would have spiraled towards SgrA⋆, and IRS 13E would be its remnant. Furthermore, IRS 13E might be the second black hole needed according to a model by Hansen & Milosavljević (2003) to drag massive main-sequence stars, in the required timescale, very close to the massive black hole. The detection of a discrete X-ray emission (Baganoff et al. 2003) at the IRS 13 position (within the positional accuracy) is examined in this context.

Key words. instrumentation: adaptive optics – infrared: stars – Galaxy: center – stars: Wolf-Rayet

1. Introduction

In the early images of the central region of the GC recorded in the near infrared, at the best seeing-limited resolution, several bright point sources dominate the ~20″ × 20″ field centered on SgrA⋆. With the radical improvement of angular resolution through multiple short exposures with shift-and-add (SHARP camera, Eckart et al. 1995) or speckle techniques (Ghez et al. 1999), with the images from the NICMOS cameras on board HST (Stolovy et al. 1999), to the advent of adaptive optics correctors behind large telescopes as NAOS (Ott et al. 2003), a more complex vision of this crowded field has emerged. At a spatial resolution in the best case of 0.05″ (Ghez et al. 1999) new, faint stellar sources appear and the early-identified sources are often resolved into several components. Therefore, the observed spectra, generally made at a resolution limited at best by a slit not less than 1″ wide, are actually composites of emission from stellar objects of different spectral type as well as from emission lines from the surrounding interstellar medium (ISM). The stellar type identified from these spectra can be wrong if attributed to a single source, which can erroneously look unusual. This care led to the paper on the revised identifications of the central cluster of He I stars by Paumard et al. (2001) made from slitless integral field spectroscopy, with BEAR an imaging Fourier Transform Spectrometer (Maillard 2000). This instrument makes it

⋆ This paper is based on observations obtained with the Adaptive Optics System Hokupa'a/Quirc, developed and operated by the University of Hawaii Adaptive Optics Group, with support from the National Science Foundation.

⋆⋆ On observations obtained with the Canada-France-Hawaii Telescope, operated by the National Research Council of Canada, le Centre National de la Recherche Scientifique of France and the University of Hawaii.

possible to obtain near-infrared spectroscopy at the seeing-limited resolution of Mauna Kea (i.e. ≃0.5″), which represents a significant improvement. However, this resolution is not sufficient for such a crowded field. Therefore, the data were compared to adaptive optics (AO) images in the K band of the same field, with a spatial resolution of ∼0.15″, in order to check whether the emission sources at the angular resolution of seeing were single stars or not.

Among the sources studied in this paper the object historically named IRS 13, is a typical example. Located approximately 3.6″ south-west of SgrA⋆, at the edge of the circular structure of the SgrA West HII region called the Minicavity, it appears in early works at near-infrared wavelengths, in J, H, K (Rieke et al. 1989) and L (Allen & Sanders 1986), as a bright spot. However, from a discussion on the sources of energy at the Galactic Center, Rieke et al. (1989) note "there are separate luminosity sources in the core of the 10 μm sources 1, 9 and 13", because, particularly for IRS 13, the energy distribution from 1 to 5 μm presents a sudden, steep increase beyond 3 μm. A first work at subarcsecond resolution, by lunar occultation in the K band (Simon et al. 1990), indicates that IRS 13 resolves into a pair of sources, separated by ∼1.2″, which were henceforth designated as IRS 13E and 13W. In the photometric survey of Ott et al. (1999) from SHARP imaging data (Eckart et al. 1995), at a limit of resolution of ∼0.15″ obtained by deconvolution, two equally bright components ($K_{\rm mag}$ = 10.26) are reported, IRS 13E1 and 13E2, with a separation of 0.2″. Paumard et al. (2001) published the first AO map of IRS 13E in the K band, extracted from a larger image of the central region obtained with the CFHT-AO system (Lai et al. 1997). We noted that a fainter third source, we called IRS 13E3, was also present, forming a kind of equilateral triangle with 13E1 and 13E2. In parallel, Clénet et al. (2001) published a photometric analysis of the same data. For IRS 13E they reported three components in the K band, noted 13E1, 13E2 and 13N. From the given offset coordinates the source called 13N in this paper is not exactly coincident with the source we had previously called 13E3 (Paumard et al. 2001).

In the meantime, spectroscopic works on the stellar population of the central parsec were conducted. Several spectra of IRS 13 (Blum et al. 1995; Libonate et al. 1995; Tamblyn et al. 1996), and specifically of IRS 13E (Krabbe et al. 1995; Genzel et al. 1996; Najarro et al. 1997), and of IRS 13W (Krabbe et al. 1995) have been published. They cover mostly the K band, i.e. all or part of the 1.95−2.45 μm range, and one the 1.57−1.75 μm region of the H band (Libonate et al. 1995). From these spectra IRS 13W is unambiguously a cool star with the strong vib-rot CO signatures at 2.3 μm. Emission lines were detected on IRS 13E, typical of a luminous, hot star: strong He I 2.058, 2.112 μm, Brγ line and other Brackett lines up to Br12, plus weaker lines of [Fe II], [Fe III], and a weak emission at 2.189 μm attributed to He II. The 7−10 line is the most intense of this ion in the K band, and is supposed unblended, while the 8−14 line cannot be distinguished from Brγ of which it is separated by less than 2 cm^{-1}. The He II line if detected is a precious type indicator in the classification of WR stars (Tamblyn et al. 1996; Figer et al. 1997). From these spectral characteristics Libonate et al. (1995) concluded "the IRS 13 spectrum bears a strong resemblance to the low-resolution K-band spectra of P Cygni (a LBV) and the AF source". Krabbe et al. (1995) proposed IRS 13E as a WN9 star. From a K-band spectrum of the Minicavity Lutz et al. (1993) attributed to [Fe III] several emission lines (2.145, 2.218, 2.242, 2.348 μm). Images at 2.218 μm show that this line is present all over the Minicavity, with a particular enhancement at the position of IRS 13. From NICMOS data in the *F164N* filter (Stolovy et al. 1999) the lower ionized Fe species, [Fe II] is detected in emission in the central ISM, particularly strong at the edge of the Minicavity, but remarkably absent at the position of IRS 13E. As mentioned in this paper the ionization condition for [Fe III] requires 16.2 eV while only 7.2 eV are required for [Fe II]. Hard ionization radiation is likely originating from IRS 13E. Hence, it can concluded that these iron lines are not of stellar origin but are present in the surrounding ionized gas.

From the extraction of the He I 2.058 μm line profile at high spectral resolution from the BEAR data, Paumard et al. (2001) concluded that one of the three sources identified as forming IRS 13E, instead of a LBV-type star should be already at the WR stage. The main argument was the width of the observed emission line profile ($FWHM \simeq 974$ km s^{-1}), typical of WR stars, making the source belonging to a class of broad-line stars including 8 other stars in the central cluster of helium stars. It was also measured that the broad-line stars were in average weaker by ≃2.4 mag in the K band than the rest of helium sources which were characterized by a narrow He I emission line. With a $K_{\rm mag}$ for IRS 13E3 consistent with the magnitude measured for the other broad-line stars, and 13E1 and 13E2 much brighter, it was proposed that IRS 13E3 should be the WR-type helium emitter. It was not possible to precise the 13E1 and 13E2 stellar type.

In the centimetric domain, Zhao & Goss (1998) presented the detection of IRS 13 at 7 and 13 mm with the VLA, at a resolution of 0.06″, which they reported to be the brightest radio continuum source after SgrA⋆ at the Galactic Center. They resolved the source into two components, one with no significant proper motion while the other one is moving south at a rate 6.2 ± 1.1 mas yr^{-1}. They called the two compact H II regions IRS 13E and IRS 13W, which was improper, since these denominations had already been given to infrared sources at IRS 13 as reminded above, with which they are not coincident. However, this detection is another element which makes this source special.

The detection of a bright, discrete X-ray emission source (Baganoff et al. 2003; Muno et al. 2003) at the IRS 13 position within the positional accuracy – source CXOGC J174539.7-290029 – among the brightest sources within the central parsec besides SgrA⋆, is a last element contributing to make this source an object of interest. This coincidence already triggered the interest of Coker et al. (2002) who presented the first Chandra X-ray spectrum of IRS 13 and deduced that it was consistent with a highly absorbed X-ray binary system. They concluded that IRS 13E2 should be a compact post-LBV binary whose colliding winds were the source of the X-ray emission.

As a conclusion, the origin of the brightness of IRS 13, one of the brightest objects at all wavelengths in the vicinity of SgrA*, has been a matter of debate. We examined all the high-angular resolution images in the near infrared currently available. This analysis made it possible to build a completely new picture of IRS 13 which is presented in this paper. We will show that the peculiar spectral energy distribution (SED) previously reported is well explained by the nature of the individual sources which compose IRS 13. Unexpectedly, this analysis provides new insight to the unsolved question of the formation of the central massive cluster. It has also given the opportunity through the study of the stars in the IRS 13 field to characterize a sample of the star population in the central parsec. A preliminary version of the paper was presented at the Galactic Center Workshop 2002 (Maillard et al. 2003).

2. High-angular resolution images of IRS 13 and data reduction

Ground-based AO images from several telescopes and space-based NICMOS data containing IRS 13 in their field have been gathered. Their characteristics are given in Table 1.

2.1. Adaptive optics data

We have analyzed data from three different AO systems: PUEO/CFHT (Lai et al. 1997), Hokupa'a/Gemini North (Graves et al. 1998), and Adonis/ESO 3.6-m telescope (Beuzit et al. 1997). The CFHT data, in the *K* band, were obtained on 26 June, 1998. They were already presented and analyzed in detail in Paumard et al. (2001). The total field covers $40'' \times 40''$ centered on SgrA*. The *FWHM* of the Point Spread Function (PSF) varies from $0.13''$ to $0.20''$ in the field since PUEO has a visible wavefront sensor, requiring to use a $V \simeq 14$ star $20''$ to the north-east of the field center. The *L*-band data were obtained with the ADONIS visible wavefront sensor in 2000, from 20 to 22 May, on the ESO 3.6-m telescope. These data are described in Clénet et al. (2001). The final *L*-band image we used has a PSF with a *FWHM* of $0.291''$ and covers a field of $\simeq 13'' \times 13''$ centered on SgrA*. The Gemini North data were part of the AO demonstration run conducted by F. Rigaut on the Galactic Center in July 2000. The data were obtained with the Hokupa'a AO system and the QUIRC camera (Graves et al. 1998) in the *K*p and the *H* band (Table 1) respectively 3 and 6 July in field 1, centered on SgrA*. The field coverage of each image is $20'' \times 20''$. For the *H* image the *FWHM* of the PSF varies from 0.115 to $0.19''$ and for the *K*p image from 0.12 to $0.18''$. In the vicinity of IRS 13 the measured *FWHM*s are respectively $0.180''$ and $0.172''$. These AO data are characterized by a low Strehl ratio of 2.5% in *H* and 7% in *K*p. The small portion of the AO image in the *K*p filter analyzed in the paper is shown in Fig. 1.

2.2. NICMOS data

Six filters, coded *F110M*, *F145M*, *F160W*, *F187N*, *F190N*, and *F222M* were used in observing the stars in the inner parsec of the Galactic Center with the NICMOS cameras on board HST, as part of three independent Galactic Center programs (7214, 7225, and 7842). These data were taken between Aug. 1997 and Aug. 1998. The filter properties (central wavelength, bandwidth, zero-magnitude flux, pixel size) and the data processing of the raw data are described in Rieke (1999) and Stolovy et al. (1999). Although each program covered a larger region, we extracted a small portion of $\simeq 4'' \times 4''$ centered on IRS 13E of the image from each filter. All these diffraction-limited images were particularly useful to derive the SED of the stellar components of IRS 13 and its environment.

Apart from wide (W) or medium (M) bandpass filters, *F187N* is a 1% narrow-band filter centered on the Paα line. By subtraction of *F190N*, a comparable narrow-band filter in the nearby continuum, the distribution of the ionized gas in the inner parsecs was obtained (Stolovy et al. 1999). In this map are also discrete emission sources which must come from Paα emission in the atmosphere of hot stars. We used a best-fit scale factor between *F187N* and *F190N* in order to minimize both positive and negative stellar residuals of the stars in the central parsec. Negative residuals can arise in stars with Paα absorption and/or in stars with local excess extinction along the line of sight. For this paper, we identified emission line stars as those with very significant *F187N/F190N* ratios (exceeding 1.2). The portion of the resulting Paα image with the IRS 13 complex was essential in determining which of the individual stars was an emission line star (Fig. 3).

Table 1. Instruments, filter properties and year of data acquisition of the high-resolution images of the IRS 13 field.

Filter	Instrument/Telescope	$\lambda/\Delta\lambda$ (μm)	Year
F110M	NICMOS/HST	1.10/0.200	97–98
F145M	NICMOS/HST	1.45/0.197	97–98
F160W	NICMOS/HST	1.60/0.400	97–98
H	Hokupa'a+Quirc/Gemini N	1.65/0.296	2000
Paα	NICMOS/HST	1.87/0.019	97–98
F190N	NICMOS/HST	1.90/0.017	97–98
*K*p	Hokupa'a+Quirc/Gemini N	2.12/0.410	2000
K	PUEO+KIR/CFHT	2.20/0.340	1998
F222M	NICMOS/HST	2.22/0.143	97–98
L	ADONIS+COMIC/3.6 m ESO	3.48/0.590	2000

2.3. Data reduction

The initial processing of each dataset is not described here. It can be found in the papers cited with the presentation of each of them. Below are listed the main operations which were performed subsequently to the initial data reduction.

2.3.1. Methods of star extraction

To perform the extraction of the individual stars from the AO and NICMOS data, *StarFinder*, an IDL procedure (Diolaiti et al. 2000) specially written for AO data, was first used.

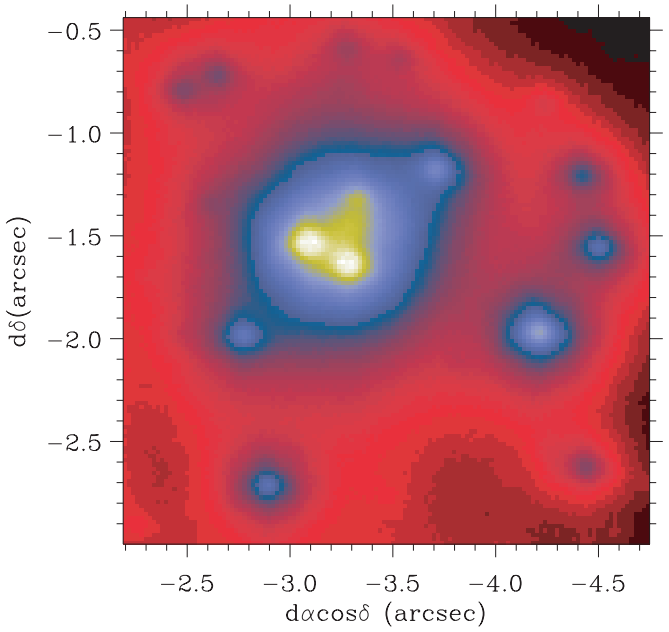

Fig. 1. IRS 13 field from the Gemini AO image in the *K*p band. IRS 13E is the central, compact group of stars and IRS 13W the brightest source ∼1″ southwest of IRS 13E. The coordinates are in arcsec offset from SgrA⋆.

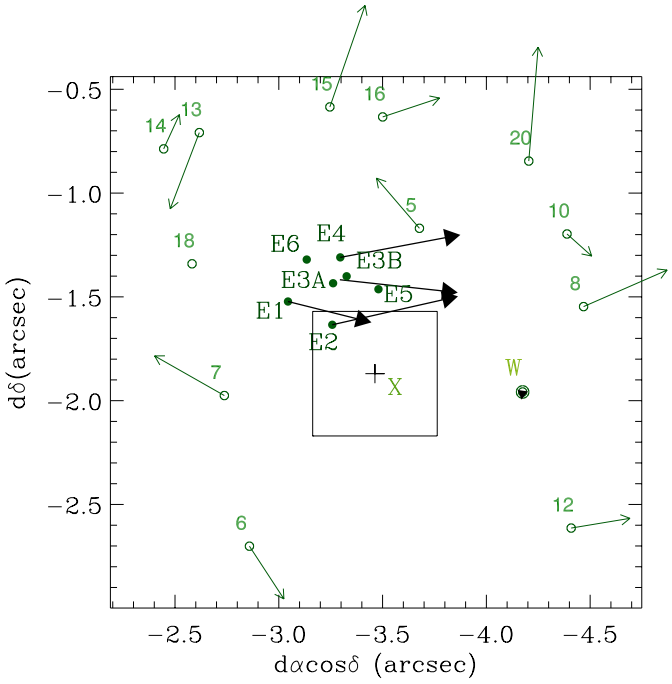

Fig. 2. The Fig. 1 field with the star detected after deconvolution by the MCS code (Sect. 2.3). The vector associated with most of the stars represents in amplitude the velocity and the direction of proper motions measured from SHARP data by Ott et al. (2003). For E3A and E3B, only the proper motion of the center of light is determined. The amplitudes reported in Table 6 for the four brightest sources of IRS 13E give the scale of the proper motion vectors. The cross marked X represents the nominal position of the X-ray source at the center of an error box of ±0.3″(see Sect. 3.2).

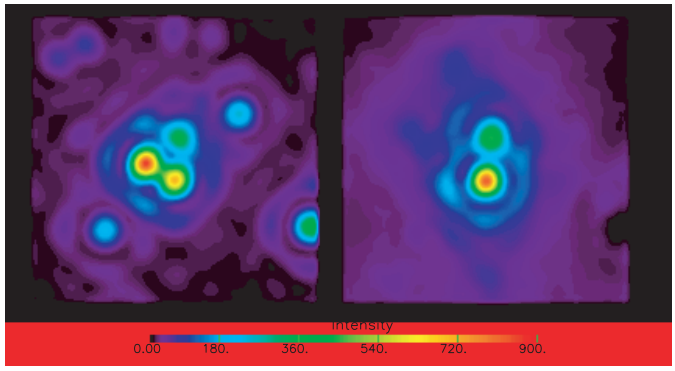

Fig. 3. At left, NICMOS images of IRS 13E in the Paα filter (1.87 μm), and at right, difference between this image and the suitably scaled image in the continuum at 1.90 μm. Only IRS 13E2 and IRS 13E4 remain which appear as emission line stars.

The preliminary operation consists of building a good PSF by averaging several isolated and bright stars in each image. By adjusting the PSF to the local peaks in the field the exact position and the flux of the corresponding stars are retrieved by the procedure.

The image residuals left by applying this procedure led us to suspect that more sources might be present in the IRS 13 complex, which could not be detected because the spatial resolution was not high enough to separate them. To improve the star detection we applied a new deconvolution code called MCS (Magain et al. 1998). Contrary to the *StarFinder* procedure, the MCS program uses an analytical PSF (a Moffat-type function). The final PSF is chosen prior to deconvolution, with a width compatible with the original image sampling. Thus, the final PSF can be narrower than the observed one without violating the Shannon sampling theorem. The contribution of a continuous background is also matched to the image with an adjustable smoothing. The sampling was high enough for the Gemini AO images, in the *H* and the *K*p bands, to provide a substantial gain in resolution. Because of the sampling of the *L*-band image a more limited gain was obtained, which was useful anyway. For the *H* and the *K*p images the width of the synthetic PSF is equal to 0.040″ and to 0.192″ for the *L*-band image, i.e. a gain in resolution respectively of a factor 4.5 in *H*, 4.3 in *K*p and 1.5 in *L*. However, this method applied to the IRS 13 images demanded many trials to reach a stable and plausible solution because of the presence of a non uniform background in which the sources are embedded. The convergence was helped by the comparison between the solutions for the *H* and *K*p filters. We imposed the sources to be detected in both bands, to avoid the risk of taking deconvolution artifacts for sources. The two filter bandpasses are almost adjacent which makes pertinent the detection in both filters, even for very red or very blue objects. This code was not applied to the CFHT *K*-band nor to the NICMOS images, which both PSFs show significant secondary rings, because they are not correctly handled by this code, written for seeing-limited images. Anyway, it was applied on the Gemini/Hokupa'a data because of their low Strehl ratio.

2.3.2. Calibration

All the NICMOS data were calibrated as described by Rieke (1999). The calibration of the sources in the L band was based on the photometry of IRS 13W reported by Clénet et al. (2001), a prominent, isolated source in this band. The Gemini data in the H and the Kp filters were not calibrated. In order to minimize photometric uncertainties between data from various origins we calibrated the two filters by interpolation from the NICMOS data which offer a set of filters close to H and Kp. Based on IRS 13E1, a bright and well-measured star by MCS deconvolution in the stellar complex, and taking into account the exact filter bandpasses, we applied a strict linear interpolation between the *F160W* and *F190N* flux of this star for the H band (central wavelength 1.65 μm), between *F190N* and *F222M* for the Kp band (central wavelength 2.12 μm, see Table 1). With this source calibrated that way in the H and the Kp filters the flux measurements of all the other sources in the two filters were calibrated. The intensities of the detected sources in the 8 filters were expressed in μJy as were originally the NICMOS data.

2.3.3. Proper motions

We obtained from Ott et al. (2003), who have conducted an analysis of ten years of SHARP data, providing more than 1000 proper motions in the central parsec, the proper motions of the main components of IRS 13 and of its nearby field.

2.4. BEAR data

Even though the BEAR data are not at the spatial resolution of the NICMOS and AO data, the Brγ and 2.06 μm He I line profile at IRS 13E were used as complementary information to help determine the spectral type of the underlying stars. The IRS 13 complex is located in a region of interstellar emission, intense in Brγ (Morris & Maillard 2000; Paumard et al. 2003a) as well as in the 2.06 μm helium line (Paumard et al. 2001). Hence, the line profiles had to be corrected to remove the ISM contribution, made here of two main velocity components (Fig. 4 – central panel), superimposed to the stellar profile. This operation required special attention for the Brγ profile since the ISM emission is locally very intense. Only the high resolution (21.3 km s^{-1}) made it possible to separate, with some approximation anyway, the stellar profile which is naturally broader, from the interstellar components.

3. Results

From the 8 high-resolution images between 1.1 and 3.5 μm (Table 1) and the spectroscopic data available, the following results on the IRS 13 complex and its environment have been obtained:

3.1. Star detection

Twenty sources in total (Table 2) are detected both in H and Kp after MCS deconvolution of the Gemini data in the small IRS 13 field, which are identified in Fig. 2. All these sources were searched for with *StarFinder* for the filters where the deconvolution operation could not be applied, and again with the MCS code in the L band. Empty positions in Table 2 indicate that the source is not detectable in a specific filter. An upper limit is given at some positions for the extreme filters (1.1 μm and L) where the detection is the most difficult. This limit is not uniform in the field depending on the proximity of another bright source, particularly in L.

Table 2. Photometric measurements in all the filters, in log (μJy), of all the stars detected by MCS deconvolution (Sect. 2.3) of the 2.5″ × 2.5″ IRS 13 field from the H and Kp Gemini AO images. Measurements in the NICMOS filters (F) were obtained by *StarFinder*, and in the L band by MCS analysis. The sources are listed by order of decreasing brightness in the Kp band, except IRS 13W, which is listed first. Values preceded by < in the 1.1 μm and the L bands are minima of detection, i.e. flux upper limits.

ID	*F110M*	*F145M*	*F160W*	*H*	*F190N*	*K*p	*F222M*	*L*
W	<0.56	2.58	3.28	3.20	3.96	4.27	4.36	4.89
E1	1.76	3.40	3.82	3.93	4.27	4.40	4.49	5.03
E2	1.61	3.22	3.71	3.80	4.17	4.38	4.48	5.37
E4	0.93	2.68	3.17	3.28	3.69	4.11	4.18	<4.66
5	0.78	2.66	3.20	3.30	3.72	4.04	3.93	
6	0.39	2.51	3.07	3.14	3.57	3.94	3.89	
7	1.23	2.78	3.20	3.26	3.63	3.92	3.88	
8	0.62	2.55	3.08	3.08	3.53	3.90	3.81	
E3A	<0.45		2.29	2.43	3.11	3.81		5.46
10	0.11	1.88	2.63	2.81	3.23	3.68	3.55	
E3B	<0.45		2.11	2.24		3.57		5.29
12	0.69	1.98	2.62	2.66	3.15	3.48	3.45	
13	−0.09	2.02	2.58	2.65	3.14	3.46	3.40	
14	−0.16	2.01	2.55	2.65	3.11	3.43	3.34	
15	−0.06	1.75	2.25	2.37	2.82	3.12	3.23	
16		1.57	2.18	2.36	2.71	3.11	2.92	
E5	<–0.17	1.60		1.75	2.72	3.08	3.61	5.07
18	0.56	1.87	2.27	2.30	2.74	2.99	3.02	
E6	<0.48		2.46	2.53		2.97		<4.68
20	0.86	1.42	2.01	2.11	2.57	2.88	2.89	

In conclusion, IRS 13E is resolved into a compact cluster of at least 7 objects encircled within ≃0.5″ (Fig. 2). The two brightest sources, 13E1 and 13E2, had already been identified in Ott et al. (1999) and in Paumard et al. (2001). The one we had noted 13E3 appears double after deconvolution. Thus, we call the two components 13E3A and 13E3B. By continuity, the closest bright source, north of 13E3, is called 13E4. Two other sources revealed by deconvolution are called 13E5 and 13E6.

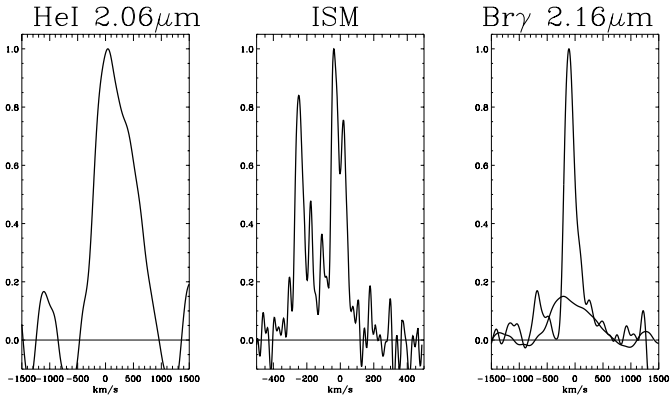

Fig. 4. He I 2.06 μm and Brγ emission line profiles at IRS 13E normalized to 1, from the BEAR data, after subtraction of the interstellar emission (ISM) contribution the observed profiles. The difference of linewidth is noticeable. The multi-component ISM emission, extracted from a ring around IRS 13E in the Brγ data cube, is shown in the middle panel. Since He I 2.06 μm is coming only from 13E2 (Clénet et al. 2003) the broad profile adjusted on the wings of the Brγ profile, of same width as the He I profile, shows the relative intensity of Brγ from 13E2 compared to 13E4.

3.2. Astrometry

The positions of the sources in the 2.5″ × 2.5″ IRS 13 field in offsets from SgrA⋆ are given in Table 3. The astrometry was retrieved from the results of the deconvolution of the portion of the Gemini *K*p-band image. The precision of the positions depends on the brightness of the sources. For the brightest sources the relative 1-σ position error is equal to 1.0 mas. From these positions the projected angular separations between the main IRS 13E components are given in Table 4, translated to AU, by taking a distance to the GC of 8 kpc (Reid 1993). All the sources of the small field are detected by the reprocessing of the SHARP data we obtained prior to publication from Ott et al. (2003), except that a single source is given for E3A and E3B (#118) and E6 is not detected. Table 3 offsets are estimated from the positions of isolated stars around IRS 13E published by Ott et al. (1999) which, in this paper are given relative to IRS 7. The offset of IRS 7 from SgrA⋆ estimated from VLA measurements, taken from Menten et al. (1997) is added. The identification of the sources is presented in Fig. 2.

We used this astrometry to examine the position of the X-ray source CXOGC J174539.7-290029 whose IRS 13 is proposed as the optical counterpart by Baganoff et al. (2003). The X-ray source was placed in Fig. 2 by estimating the offset of the source with respect to SgrA⋆ from the coordinates of both sources reported in Baganoff et al. The 1-σ error reported on the coordinates of each X-ray source is of ±0.2″ in right ascension and ±0.1″ in declination. By combining the astrometric uncertainties on the two source positions we drew a minimum error box of ±0.3″ around the nominal position. The resulting position falls outside the center of IRS 13E, which will be discussed in Sect. 6.

Table 3. Offsets from SgrA⋆[a] of the sources shown in Fig. 2.

ID	ID'[b]	$\Delta\alpha\cos\delta$(″)	$\Delta\delta$(″)
W	40	−4.17	−1.96
E1	25	−3.02	−1.58
E2	27	−3.24	−1.68
E4	77	−3.26	−1.35
5	69	−3.64	−1.20
6	101	−2.90	−2.77
7	114	−2.74	−2.05
8	120	−4.45	−1.53
E3A	118	−3.24	−1.48
10	145	−4.35	−1.19
E3B	118	−3.30	−1.44
12	188	−4.44	−2.60
13	296	−2.56	−0.79
14	295	−2.39	−0.88
15	328	−3.18	−0.63
16	381	−3.44	−0.67
E5	780	−3.46	−1.50
18	902	−2.55	−1.42
E6		−3.10	−1.37
20	459	−4.15	−0.85
X		−3.44	−1.79

[a] SgrA⋆ position (Yusef-Zadeh et al. 1999):
α(2000) = 17 45 40.0383 ± 0.0007s
δ(2000) = −29 00 28.069 ± 0.014″.
[b] Identification number from Ott et al. (2003).

Table 4. Projected separation of the main IRS 13E sources. From the astrometry the precision on the distance betwen two sources is ±15 AU.

Sources	Ang. sep.	Distance (AU)
E1−E2	0.241″	1930
E1−E4	0.330″	2630
E2−E4	0.327″	2600
E2−E3A	0.200″	1600
E3A−E3B	0.073″	590

3.3. Photometry

Table 2 has been used to derive the standard photometry in *H*, *K*, and *L* bands and the color indices of all the sources identified in Fig. 2. The *K*p filter (Table 1) which is close and has a width comparable to *K* was used. It is referred to as *K* in the results presented in Table 5.

Table 5. H, K and L photometry of the IRS 13E cluster and of the nearby field stars from Table 2.

ID	H	K	L	$H-K$	$K-L$
W	14.55	11.30	8.92	3.25	2.38
E1	12.74	10.98	8.59	1.76	2.39
E2	13.05	11.03	7.73	2.02	3.30
E4	14.37	11.72		2.65	
5	14.32	11.90		2.42	
6	14.71	12.13		2.58	
7	14.41	12.18		2.23	
8	14.86	12.23		2.63	
E3A	16.48	12.47	7.50	4.01	4.97
10	15.55	12.80		2.75	
E3B	16.95	13.07	7.92	3.90	5.14
12	15.92	13.28		2.65	
13	15.95	13.35		2.60	
14	15.95	13.42		2.53	
15	16.65	14.20		2.45	
16	16.66	14.22		2.44	
E5	18.19	14.28	8.48	3.90	5.79
18	16.79	14.52		2.29	
E6	16.24	14.56		1.68	
20	17.29	14.78		2.52	

Table 6. Amplitude of proper motions of the main IRS 13E sources (from Ott et al. 2003).

Name	mas/yr	km s^{-1}
13E1	5.50	207 ± 14
13E2	8.20	310 ± 19
13E3	7.54	285 ± 270
13E4	7.77	294 ± 32

3.4. Proper motions

From the results communicated by Ott et al. (2003), the direction and amplitude of the proper motions for the main IRS 13E sources and most of the stars in the 2.5″ field are represented in Fig. 2. Note that the five sources, 13E1, 13E2, 13E3A, 13E3B (proper motion is only given for the center of light of 13E3A and B) and 13E4 are all moving West, with a similar velocity, while all the nearby stars have very different directions and amplitudes. The amplitude of the proper motions of the four main sources, in angular motion per year (for a GC distance of 8 kpc) and in velocity, are presented in Table 6. The reported uncertainties come from the mean error on the proper motion vector coordinates adjusted on the set of positions. The rms uncertainty on 13E3 proper motion is the largest one, because of the difficulty of measuring accurate positions from several epochs of SHARP data for a weak source so close to much brighter sources, 13E2 and 13E4. The error becomes large for data recorded with poor seeing conditions.

3.5. The ionized gas near IRS 13E

The Paα emission line is tracing also in the two central parsecs the HII region called SgrA West or commonly the Minispiral. IRS 13E is located just at the northern end of a bright emission arc, part of the circular structure open toward SgrA*, called the Minicavity. In Stolovy et al. (1999) the bubble-like feature is proposed as created by the wind from a star identified by a weak Paα point source, since located very near the geometric center of the Minicavity. A proper motion of the edge of the Minicavity of ∼200 km s^{-1} is measured by Zhao & Goss (1998). In Paumard et al. (2003a), it is shown that the Minicavity is embedded inside a non-planar gas flow of the Minispiral, called the Northern Arm. In the field of the Minicavity another velocity structure is identified, stretched toward northwest, called the Bar, roughly perpendicular to the bright edge of the Northern Arm. On the line of sight of IRS 13E these two velocity structures produce the two main components in the line profile of the ionized gas shown in Fig. 4 central panel. The fastest component at −250 km s^{-1} is due to the motion of the gas disturbed by the Minicavity, and the slowest component, at −39 km s^{-1}, to the Bar. On a morphological basis IRS 13E would seem to belong to the bright arc of the gas shocked at the edge of the Minicavity. On the intensity map of the Bar, isolated by this multi-component analysis, a small region just centered on the IRS 13E position appears locally enhanced. Therefore, the observed brightness of the ionized gas around the position of IRS 13E is due to the addition of two contributions on the line of sight: the edge of the Minicavity and the locally excited gas of the Bar. Only this latter component is due to the presence of the IRS 13E sources, by their strong ionizing flux. Hence, IRS13E should be located close to or inside the Bar, which lays behind the Minicavity (Paumard et al. 2003a).

3.6. The stellar Paα emission line

As shown in Fig. 3, only two of the IRS 13E components, IRS 13E2 and 13E4, remain after subtraction of the *F190N* continuum from the *F187N* filter which contains Paα. These two stars are unambiguously emission line objects, with the integrated line intensity at IRS 13E2 brighter by a factor 2.35 ± 0.1 than at IRS 13E4.

3.7. The Brγ and the He I 2.058 μm line profiles

The profiles of these two emission lines were obtained from spectra extracted on the same aperture size (3 × 3 pixels i.e. ≃1″ × 1″) from each BEAR data cube, at the IRS 13E position. With the spatial resolution of the BEAR data the contribution of the two emission line stars 13E2 and 13E4 is mixed, to which is added the ISM emission. After the most plausible subtraction to each line profile of this latter contribution, shown on the central panel of Fig. 4, possible thanks to the spectral resolution of the data, Brγ appears much narrower than the He I 2.06 μm line. With a *FWHM* of 215 km s^{-1}, compared to ∼900 km s^{-1} for the helium line, as already measured in

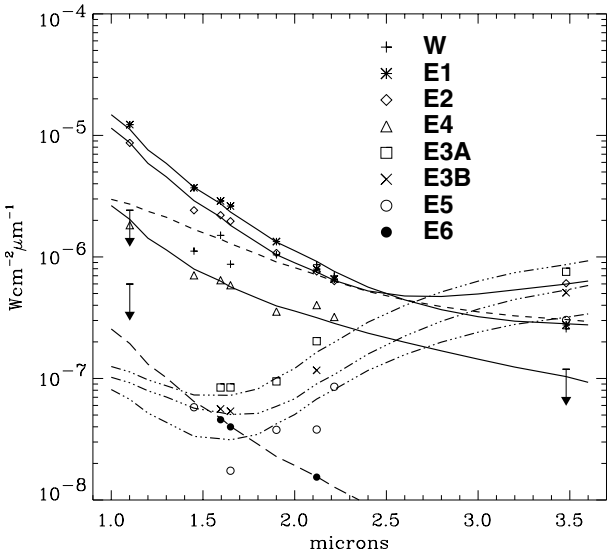

Fig. 5. Dereddened SED of the IRS 13 sources in W cm^{-2} μm^{-1}. The top of the arrows indicates the estimated upper limit of the detectable flux in the 1.1 μm and the L-band filters. The various lines represent the best fit between 1 and 4 μm of the data points from a two-component model with the parameters of Table 7 and the most adapted A_v values.

Paumard et al. (2001), the two lines should belong to two different sources, which is discussed in Sect. 4.2.

3.8. Spectral energy distribution and extinction law

The photometric measurements presented in Table 2 were used to build the SED between 1 and 4 μm of the IRS 13 components (Fig. 5), and also of all the stars detected in the surrounding field. To achieve the final goal of determining the spectral type of these stars, a dereddening has to be applied over this range. The extinction over the central parsecs is highly variable (Blum et al. 1996; Rieke 1999; Scoville et al. 2003). We took the most recently published law, which is a merging of previous works (Moneti et al. 2001), and adjusted A_v, making first the simplifying assumption that the reddening toward IRS 13E and the few arcsecs around would be identical for all the sources. For this adjustment we were helped by two constraints: IRS 13E2 and 13E4 are emission line sources (Fig. 3), therefore hot sources with a blue SED, while IRS 13W is a cool star (Krabbe et al. 1995). Black-body curves were fitted to the data. A_v was adjusted in order to fulfill the two constraints. Higher values of A_v make the sources bluer, while lower values make the sources redder. Temperatures higher than 25 000 K had to be introduced for IRS 13E1, 13E2 and 13E4, which correspond to the Rayleigh-Jeans regime in this spectral range. In that case, only a lower limit of $T_{\rm eff}$ can be derived. The slope of the SED becomes constant in a log [F(λ)] diagram. For these stars the adjustment of A_v makes it possible to bring the SED parallel to the data points, providing the strongest constraint on A_v. Finally, a value of $A_v = 35 \pm 0.5$ was adopted from the three hot stars, 13E1, 13E2 and 13E4. A mean value of $A_v = 30.5$ had been determined by Rieke (1999) from a survey of the stars in the central parsec, which excluded objects like IRS 13 from the color–magnitude diagram because of the surrounding dust. We confirm a much higher A_v value for IRS 13E. On the other hand, for IRS 13E6 $A_v = 35$ was too high for a good fit to the data. A value of 29 was more appropriate. On the contrary, we will show in Sect. 4.7 that a value of $A_v = 38.5$ had to be adopted for IRS 13W.

However, it appeared that the fit of the dereddened data from Table 2 was not possible with a single temperature for the IRS 13 sources. Except 13E6, they show an infrared excess. Then, the fit was made as a sum of two black-body curves, $Coef_1 \times BB(T_1) + Coef_2 \times BB(T_2)$. The four parameters of adjustment obtained for each star are reported in Table 7. The final SEDs are shown in Fig. 5. From all the results presented above a spectral classification of the stars detected in the IRS 13E cluster is proposed.

Table 7. Fitting parameters of the SED of the IRS 13 sources. The spectral type of each source, as discussed in Sect. 4, is summarized in the last column.

Star	$Coef_1$	T_1 K	$Coef_2$	T_2 K	A_v	Sp. type
W	13.50	3600	4250	640	38.5	M3III
E1	0.800	≥25 000	12 000	550	35	∼O5I
E2	0.620	≥25 000	40 000	550	35	∼WN8
E4	0.140	≥25 000	45	1550	35	∼O5IIIe
E3A	0.460	3800	33 000	610	35	d. WR[a]
E3B	0.375	3800	29 000	580	35	d. WR[a]
E5	0.070	6000	9800	630	35	d. WR[a]
E6	0.013	≥25 000			29	∼O5V

[a] Dusty Wolf-Rayet star.

4. Nature of the IRS 13 sources

4.1. IRS 13E1

This source is characterized by:

- no emission detected in Paα (Fig. 3);
- an elongated envelope in H and Kp toward 13E2, which shows at the star position a *FWHM* of 180 mas (to compare to the 40 mas of the PSF) or 1435 AU;
- a SED fitted by a ≥25 000 K source and an infrared excess at 550 K (Table 7);
- a $K_{\rm mag}$ of 10.9 (Table 5). At the distance of the GC and with the adopted extinction, IRS 13E1 is too luminous to be a dwarf star. A O5V star of comparable $T_{\rm eff}$ would have a $K_{\rm mag} \simeq 14$ (with $A_K \simeq 4$). IRS 13E1 is ∼3 mag brighter.

Hence, IRS 13E1 must be a blue, supergiant star. The surrounding halo of scattered emission is indicative of a strong stellar wind, which also favors the identification of a massive, hot star. Consequently, IRS 13E1 might be close to a O5I spectral type. However, at the position of the source there is no evidence in the Paα image of a negative level (Fig. 3), which would be the signature of the photospheric hydrogen line in absorption since no emission is detected. Possibly, with the uncertainty on

the adjustment of the continuum subtraction from the 1.87 μm filter, the integrated emission from the envelope in the image can be compensating the photospheric absorption. Only a near-infrared spectrum of IRS 13E1 behind adaptive optics could confirm this assumption.

4.2. IRS 13E2 and 13E4

IRS 13E2 and 13E4 are two emission line stars (Fig. 3). In the K band IRS 13E2 is brighter than IRS 13E4 by a factor $\simeq$2 (Table 5). In our L band 13E4 is no longer detectable while 13E2 can still be measured. With this detection it turns out that all the emission spectra of IRS 13E obtained up to now (see references in Introduction) are in fact the combination of two emission line stars which are likely different.

A decisive element is reported by Clénet et al. (2003). From spectro-imaging with a FP in the 2.06 μm helium line behind the CFHT-AO system they indicate that IRS 13E2 is the only helium emitter. The radical difference of linewidth between the He I 2.06 μm and Brγ stellar line profiles at IRS 13E (Fig. 4) brings another piece of information. A similar difference of linewidth of the He I 2.06 μm lines is observed among the hot stars of the central cluster (Paumard et al. 2001, 2003b), leading to the identification of two classes of massive stars. Applying this criterion to 13E2 and 13E4, and taking into account the detection of He I 2.06 μm only at IRS 13E2, it can be concluded that IRS 13E2 as a strong helium emitter with broad line is a late-type WR star, probably of WN type (Figer et al. 1999) since no detection of C III or C IV typical of WC type is reported from earlier K-band spectra. A $T_{\rm eff} \geq 25\,000$ K estimated for the source (Table 7) is consistent with this identification. IRS 13E4 with also a $T_{\rm eff} \geq 25\,000$ K (Table 7), but no helium emission, source of the narrower Brγ profile, is more likely a less evolved star than IRS 13E2. From its SED and its absolute brightness in K, fainter than IRS 13E1, IRS 13E4 can be reasonably proposed as a O5IIIe star or just reaching the LBV stage but in a high extinction phase to explain its weakness.

However, there is an apparent contradiction between the brightness of IRS 13E2 in Paα in Fig. 3 and the Brγ profile at IRS 13E from the BEAR data after correction for the ISM emission (Fig. 4). As Paα appears strong at IRS 13E2 in Fig. 3, the Brγ profile at IRS 13E should be dominated by the emission from this source and be as wide as the He I 2.06 μm profile. That is not what is observed as shown in Fig. 4. To reconcile these two facts, it must be noticed that Paα is far from a perfect indicator with narrow-band imaging technique, to distinguish between hydrogen-rich and helium-rich emitters since the Paα line (1.8751 μm) is blended with a strong helium line, He I (4–3) at 1.8697 μm. There is another helium line within the bandpass of the continuum filter, at 1.9089 μm, but which is weak and will contribute to subtract only a little of the helium emission. All these features are well seen in the CGS4 spectrum of the AF star around Paα, presented by Najarro et al. (1994), which is another helium star belonging to the class of the broad-line stars (Paumard et al. 2001, 2003b). Hence, the intensity in the *F187N–F190N* image at the star position cannot be considered as a fully reliable measurement of the true Paα emission in the stellar atmosphere. The bright spot at IRS 13E2 in Fig. 3 is likely due to the He I 1.8697 μm line and with some contribution of the Paα emission. That is consistent with the Brγ profile shown in Fig. 4 which can be decomposed into a narrow line, whose origin must be IRS 13E4, and a fainter, broad component of same width as the He I 2.06 μm line, which should be the contribution of IRS 13E2 to the observed profile. The residual Brγ profile will show a P Cyg profile, typical of hot stars with an atmosphere in expansion, consistent with the spectral type attributed to IRS E4.

4.3. IRS 13E3A and B

IRS 13E3 resolves into a double source in the deconvolved AO images in H and Kp (Fig. 2). Their projected separation is equal to $\simeq$600 AU (Table 4). The two sources are photometrically quite identical. They are extremely red objects as indicated by the measurements in Table 5, and from their SED (Fig. 5). They are faint in the H band and prominent in the L band. We measure a $K - L$ color index of $\sim$5 mag. for the two components (Table 5). Several sources in the inner parsec, mainly located along the Northern Arm (IRS 1W, 2, 3, 5, 10W, 21), are also very red objects, with $K - L > 3$, reported in Clénet et al. (2001). IRS 1W and IRS 21 have featureless spectra in the K band (Blum et al. 1996). IRS 21 has been studied in detail, from 2 to 25 μm by Tanner et al. (2002). They have fitted its SED by a two-component model, the near-infrared scattered light from the central source peaking at $\simeq$3.8 μm (760 K), and the mid-infrared re-emitted light from the dust shell at $\sim$250 K. They conclude that IRS 21 is a dusty WR star, experiencing rapid mass loss as well as the other luminous Northern Arm sources (Tanner et al. 2003). The IRS 13E3 SEDs are also fitted by two components (Table 7), but with respectively 3800 K and 600 K. IRS 13E3A and E3B are likely sources of the same type as IRS 21 and the other Northern Arm sources. The higher temperature of the infrared component can come from the additional heating of the dust shell by the very close, massive blue stars, IRS 13E1, 13E2 and 13E4. That is also consistent with IRS 13 being not a prominent source at 12.5 μm on the images in this band (Tanner et al. 2002) compared to the other Northern Arm sources.

4.4. IRS 13E5

One of the sources revealed by deconvolution of the AO images (Fig. 2) we propose to name IRS 13E5, is also present in the SHARP data (Ott et al. 2003). From the dereddened photometry (Fig. 5) this source has a SED similar to IRS 13E3A and E3B, being roughly a factor 2 fainter than each of the IRS 13E3 components. Its SED is also fitted by two thermal components, with temperatures of the same order as for 13E3A and E3B (Table 7). From this similarity we propose that IRS 13E5 is another example of dusty WR star, possibly more embedded, behind IRS 13E3A and E3B.

4.5. IRS 13E6

IRS 13E6 is detected in H, in the *F160W* filter, a broader H filter, and near the detection limit of the Kp band (Table 2) and not in L. It is not detected by Ott et al. (2003) whose data come from K-band imaging on the NTT. With $T_{\rm eff} \geq 25\,000$ K and $K_{\rm mag} = 14.56$ (Table 5) 13E6 is a weak, hot star, 3.5 mag fainter than IRS 13E1. It can be considered close to a main sequence O5V star. In Fig. 5 the best fit to the data was obtained with a value of $A_{\rm v}$ lower than for the other IRS 13E sources. It should mean that IRS 13E6 is located on the line of sight, but in front of the IRS 13E complex.

4.6. The red halo around IRS 13E

The flux in the L band is only due to continuum emission since the Brα line from the ionized gas falls outside the filter bandpass. The deconvolution of the AO image in this band, after subtraction of the stars, leaves an enhanced background emission around IRS 13E shown in Fig. 6, extending on 2″ in the North-South direction, above an almost uniform continuum. On a larger scale, over the central parsecs, a diffuse emission is seen in the mid-infrared (Tanner et al. 2002) whose structure is exactly following the intensity map of the ionized gas forming the Minispiral (Stolovy et al. 1999; Morris & Maillard 2000; Paumard et al. 2003a). This emission is the thermal emission from the dust dragged by the same fast flowing motion as the gas, heated through the trapping of Lyα photons from the central, massive star cluster (Rieke et al. 1989). In the analysis of the local structure of the interstellar gas (Sect. 3.5) we have shown that the IRS 13 complex is embedded in the flow called the Bar (Paumard et al. 2003a). This flow is also likely mixed with dust. Hence, the enhanced continuum emission seen in L around IRS 13E should come from the dust heated up by the strong UV field coming from the local concentration of hot stars. There, the emission temperature of the dust has a value around 600 K from Table 7, against 250 K at IRS 21 (Tanner et al. 2002) and probably lower out of the embedded sources. From further observations with NAOS/CONICA in the same band (Eckart et al. 2003) the bright extension 1″ north of IRS 13E resolves into a compact cluster of several very red sources. Their spectral type might be comparable to the dusty WRs as 13E3A, B and 13E5 detected next to it. Spatially-resolved spectroscopic studies are needed to confirm this hypothesis.

4.7. IRS 13W

This star is associated with IRS 13 only for historical reasons. We kept it in all the study since its cool stellar type, confirmed by the presence of CO in its K-band spectrum (Krabbe et al. 1995), was a constraint on the determination of the local value of $A_{\rm v}$. In the deconvolved Kp-band image 13W shows a larger size than the PSF which might be indicative of a dusty envelope, attested also by a significant infrared excess (Table 7). However, in the first analysis with the assumption of the same $A_{\rm v}$ value for all the IRS 13 sources a $T_{\rm eff}$ of ~2600 K was obtained for 13W. With this temperature the cool star should be of Mira-type. A $H+K$ spectrum would show the deep absorption of water vapor on each side of the K band. With the NICMOS data we have a photometric measurement at 1.90 μm, just in the water vapor band. Figure 5 shows a smooth distribution of data points. Thus, we must conclude that this temperature is too low. To increase this temperature in the fit a higher $A_{\rm v}$ value must be assumed locally. With the four parameters of the fit (Table 7) plus $A_{\rm v}$ the solution is not unique. A plausible solution is obtained with $A_{\rm v} = 38.5$ and $T_{\rm eff} = 3600$ K. A higher temperature would require a higher $A_{\rm v}$ value which would become inconsistent with the non detection of IRS 13W at 1.1 μm (Table 2). With this $T_{\rm eff}$ temperature and its luminosity IRS 13W can be assumed to be a M 3 giant star.

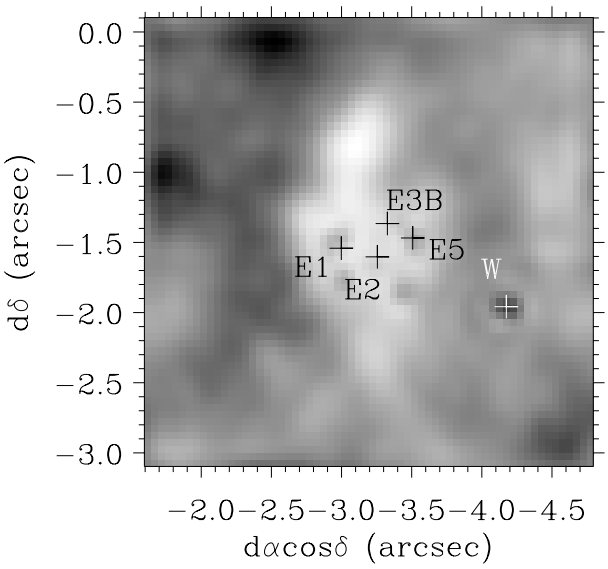

Fig. 6. Map of the residual fitted continuum in the deconvolution operation of the L-band image with the MCS code. The identified stars in this band (Table 2) have been subtracted explaining the dark holes in the map (e.g. at the W position). Source positions are marked by crosses with their names. To limit confusion, for the E3 binary only E3B position is indicated. The apparent halo might be not purely thermal emission of dust and contain more fainter embedded sources (Eckart et al. 2003). An estimation of the halo contrast is given for the brightest pixel (position −3.1″, −0.8″), which is four times brighter than east of 13E, out of the halo.

4.8. The other stars of the IRS 13 field

As presented in Table 2 twelve more stars are detected in the small field around IRS 13. Note that they are only detected in the 1−2.3 μm range. They offer an opportunity to study in detail a small sample of the central parsec stellar population. By fitting black-body curves (a single temperature component was required), under the assumption of the same $A_{\rm v}$ as for IRS 13E, nine stars are main sequence K and M stars, with $T_{\rm eff}$ from 2800 to 5000 K. Hence, they belong to the numerous old star population of the GC (Blum et al. 1996). The three remaining stars (#7, 12, 18 – Fig. 2) are very hot stars, with $T_{\rm eff} \geq 25\,000$ K and $K_{\rm mag}$ respectively of 12.2, 13.3 and 14.5 (Table 5). As proposed for IRS 13E6, they should be main sequence O stars. Near infrared spectroscopy is needed to better constrain their

spectral type. However, in this small field four out of a total of 14 sources (putting the massive components of IRS 13E apart) are apparently O-type stars, which could make a proportion of about one quarter of such stars in the central parsec, the rest being late-type stars.

5. IRS 13E as the remaining core of a massive star cluster

IRS 13E appears as only composed of hot, massive stars. This concentration within 0.5″ cannot be fortuitous. Further deep high-spatial resolution imaging could eventually reveal more components (Eckart et al. 2003). The common westward direction and similar amplitude of the proper motions with a mean value of ∼280 km s^{-1} for the main components (Sect. 3.4 and Table 6) is a decisive argument to indicate that 13E1, 13E2, 13E3A/B and 13E4 are physically bound. Regarding 13E5 for which a proper motion cannot be currently measured to associate it unambiguously to the cluster, its spectral type, identical to 13E3A/B, leads us to conclude that this source belongs to IRS 13E too. For IRS 13E6 the proper motion is not available either, but the value of A_v 6 mag lower than for IRS 13E likely indicates that the source does not belong to the cluster. The source is another O-type star, just located on the line of sight. However, in conclusion, the source historically called IRS 13E is a compact, massive star cluster with at least six members. That also means a young star cluster of a few 10^6 yr old, since several members are identified as having already reached the WR stage.

The compactness of the cluster and the common proper motion of the components raise the question of the force which keeps the massive stars bound. The hypothesis of the presence of a dark, massive source, a stellar black hole at the center of IRS 13E is natural. An intermediate-mass black hole (IMBH 10^3 to 10^4 $M_\odot$) is supposed to form by runaway growth in massive, young stellar clusters as a result of stellar collisions in the cluster center, as was modeled by Portegies Zwart & McMillan (2002). Constraints on the possible central mass could be obtained from the radial velocities of the sources. It is estimated only for the two emission line stars, with a positive velocity of ≃30 km s^{-1} for IRS 13E2 and a negative velocity of ≃30 km s^{-1} for IRS 13E4 (Fig. 4). Associated with parallel and equal proper motion vectors (Fig. 2), this suggests that both stars orbit around the center of mass in a plane orthogonal to the plane of the sky. Assuming that both stars orbit around the black hole in a symmetrical fashion on circular orbits, half the projected separation between IRS 13E2 and IRS 13E4 (Table 4) gives an orbit radius of 1300 AU/cos i where i is the angle that the line containing both stars makes with the plane of the sky. The radial velocity of each star (≃30 km s^{-1}) can be used as an estimate for their orbital velocity. A period of rotation of ≃1295 yr is derived. Then, the 3rd Kepler's law gives directly a total mass of ≃1300 $M_\odot \cos^{-1}(i) R_0/8$ kpc. We can also release the circular orbits hypothesis, and only assume that the system is bound, which means that the potential energy of each stars is greater than its kinetic energy. This gives a lower limit to the black hole mass, half the previous estimate: $M_{BH} > 750\, M_\odot \cos^{-1}(i) R_0/8$ kpc. The dependence of these two values is quadratic on the orbital velocity of the stars and linear on their distance to the black hole, so that the constraint $M_{BH} \geq 10^3\ M_\odot$ can be considered rather robust. It falls within the range derived by Portegies Zwart & McMillan (2002) for a black hole formed in the core of a dense star cluster with massive stars of initial mass ≥50 $M_\odot$.

5.1. The fate of a star cluster near SgrA⋆

The large number of massive stars in the central parsec, which are very rare elsewhere in the Galaxy, remains one of the major mysteries of this region. Since star formation would be difficult due to the strong tidal forces from the SgrA⋆ black hole, Gerhard (2001) made the interesting hypothesis that the central parsec He I stars, the most prominent of the massive young stars, might be the remains of a dissolved, young cluster, which originally formed further away from SgrA⋆. He argued that the Arches and the Quintuplet clusters, located within a projected distance of ∼30 pc from SgrA⋆, testify that star formation by cluster of massive stars has been occurring in the nuclear disk of the Galaxy. If one examines Table 7, IRS 13E appears as a kind of summary of all the spectral types of young stars observed in the central parsec from O to WR. Among the helium stars only IRS 13E appeared multiple, which motivated the current study. With the hypothesis that IRS 13E might be the remaining core of a massive star cluster, was this cluster the source of the population of massive stars observed in the central parsec?

Morris (1993) has argued that it would take longer than the lifetime of massive young stars to transport them inward within the central parsec if they formed at too large distance. The same argument is applied again by Figer et al. (2000), who claim that the SgrA⋆ cluster (Genzel et al. 1996; Ghez et al. 1999; Gezari et al. 2002) could not have formed more than 0.1 pc from the center, and then, the initial clump should have an exceptional density ≥4×10^{11} cm^3. Gerhard (2001) discarded this argument by a revision of the conditions for a cluster formed at 30 pc to spiral into the center within the lifetime of its most massive stars. The main condition is that the initial mass of the parent cloud in which the cluster forms must be massive enough (≃2×10^6 $M_\odot$) to survive the evaporation in the strong tidal field of the nuclear bulge. He concludes that clusters significantly more massive than the Arches cluster and formed a little closer than 30 pc can reach the central parsec in due time. In order to test this statement Kim & Morris (2003) have made several simulations, for different masses (10^5 $M_\odot$ and 10^6 $M_\odot$) and different initial orbit radii (2.5 to 30 pc), of the dynamical friction on a star cluster near SgrA⋆. They came to the conclusion that some simulations can be regarded as candidates for the origin of the central parsec cluster, but that "the required conditions are extreme", with an initial mass of the cluster of 10^6 $M_\odot$ or a very dense core ≥10^8 $M_\odot$ pc^{-3} (Kim et al. 2003). A mass of the cluster of 10^6 $M_\odot$ supposes a very large number of particles, with some of initial mass ≥10^2 $M_\odot$ to reach rapidly the WR stage. Compared to the relatively small number of detected helium stars, concentrated in the central parsec, ∼19 from the revision by Paumard et al. (2003b), plus few more dusty WRs,

a very large quantity of O-type stars ($>10^5$) should be detected, which is not the case from the proportion of such stars we count in the IRS 13 test field (Sect. 4.8). This might seem an argument against this scenario.

However, another analytic work by McMillan & Portegies Zwart (2003) has reconsidered the fate of a star cluster near the central dark mass. They tried to address the problem more completely by taking into account, in addition to the initial mass and the distance to the center, the original mass function of the cluster, the initial cluster radius and the stellar evolution through mass loss during the inspiral time of the cluster. They conclude that star clusters born with masses $\simeq 10^5$ $M_\odot$ within 20 pc from the center, with a half-mass radii of ~0.2 pc can reach a final distance of 1 pc within 10 Myr. As a secondary conclusion, they assess that from their mass and their distances, the Arches and the Quintuplet clusters, will never reach the vicinity of SgrA*. This latter work makes the origin of the central, massive star cluster by the dissolution of a compact cluster in the galactic tidal field more plausible, not requiring extreme mass conditions as in the simulation of Kim et al. (2003). In conclusion, we propose that the IRS 13E cluster, by its unique location and composition, is the possible core of an earlier massive star cluster, formed about 10 Myr ago, within 20 pc of SgrA*, with a mass of $\simeq 10^5$ $M_\odot$, which was the progenitor of the entire hot star population, from WR to O-type stars, observed today in the central parsecs of the Galaxy. In addition, the hypothesis of IRS 13E harboring a IMBH as consequences on this scenario.

5.2. The need for a second black hole

A recent paper by Hansen & Milosavljević (2003) came to our attention when the current work on IRS 13 was completed. The authors try to solve the difficulty of bringing disparate groups of hot stars, the WR-type stars, the LBV-type stars and the S-cluster, at their observed location within the timescale required within a single evolutionary scenario. They argue that massive star clusters can sink within the required star lifetime but are tidally disrupted at a distance greater than 1 parsec from SgrA*, from which it would result a population of sources with low binding energy orbits unlike those of the helium stars and particularly of the S-cluster stars orbiting within 0.1 pc of SgrA**. For this purpose they propose a model with an infalling IMBH. The stellar orbits continue to evolve by undergoing close encounters with the IMBH, bringing some stars near enough to be trapped by the massive BH. This model appears as a refinement of the same idea of an origin of the young star population in the central parsec as formed at a distance of the SgrA* > 10 pc where star formation can occur, in a dense star cluster sinking towards SgrA*. We propose IRS 13E with a IMBH as the possible remnant of this initial cluster.

6. What is the source of the X-ray emission at IRS 13?

The origin of the X-ray emission at IRS 13 reported by Baganoff et al. (2003) for the position, by Coker et al. (2002) for the spectrum, and by Muno et al. (2003) for complementary data on the energy distribution, must be examined in the context of the nature of IRS 13E presented in the current work. According to Baganoff et al. the X-ray source is located 0.56″ northeast of IRS 13W. Using our own astrometry (Table 3) and the offset of the IRS 13 X-ray source from the X-ray source at SgrA*, the source falls 0.75″ east of IRS 13W (Fig. 2). With some minor difference we agree that the nominal position of the X-ray source does not coincide with the center of IRS 13E (our position is 0.37″ south). This discrepancy is larger than the error box on the X-ray source. Then, the source is apparently not coincident with either IRS 13E2 as a post-LBV binary as originally proposed by Coker et al. (2002), or the IRS 13E cluster itself, which would have been the most plausible candidate with its rare concentration of several massive, hot stars with high mass loss and very fast winds, and possibly with a black hole at its center. Except a better astrometry the source CXOGC J174539.7-290029 must be considered as a source independent of IRS 13E. A systematic X-ray survey of the Galactic Center region at sub-arcsecond scale with Chandra by Muno et al. (2003) over a field of $17' \times 17'$ centered on SgrA* has revealed more than 2000 discrete X-ray sources. Stellar remnants, white dwarfs with magnetically accreting disks, binaries with neutron stars or solar-mass black holes are considered as responsible for a large fraction of these discrete sources. Such a source, too weak in the near infrared to be detected, could be present on the line of sight of IRS 13, since as measured by Muno et al. (2003) the distribution of the density of discrete sources peaks in the central parsec. The binary explanation for many stellar X-ray sources is based on a distinct emission feature centered at ~6.7 keV and otherwise a featureless spectrum. The spectrum presented by Coker et al. (2002) stops at 6 keV, probably because no energy was detected beyond, but it shows a narrow emission line at 3 keV. Wang et al. (2002) indicate that this line should be due to the contribution of massive stars. Hence, the infrared counterpart to the X-ray source could be detected by deeper spectrophotometry of the IRS 13 field. A good S/N ratio X-ray spectrum of the so-called IRS 13 source would also help to better constrain the nature of this source.

7. Conclusion

The presence of a compact star cluster of six hot, massive stars at the position of IRS 13E from high-resolution near-infrared observations is demonstrated. The spectral types of the various members range from O to WR, including dusty WRs. Proper motion measurements indicate that the brightest stars are comoving suggesting that the members of the cluster are bound by a central IMBH with a mass ≥1300 $M_\odot$. Such a secondary black-hole in the vicinity of SgrA* could be the element needed to explain the population of massive young stars observed today (Hansen & Milosavljević 2003).

To precise the spectral type of the components, better constrain the mass of the IMBH, spectroscopy in the $1-5\,\mu$m range of all the individual sources within IRS 13E, at angular resolution as good as 0.1″, is required. In the L and M bands it should confirm the expected featureless spectrum, except dust

signatures, of the IRS 13E3 and 13E5 objects. These studies will need near-infrared 3D spectrometers behind an AO system on a 8-m telescope, like SINFONI (Mengel et al. 2000 and AMBER behind VLTI (Petrov et al. 2000). Deeper AO imaging, as already obtained with NAOS/CONICA north of the IRS 13E center (Eckart et al. 2003), could make it possible to detect more members of the cluster. Proper motions of the fainter members would help to confirm which of the individual sources are kinematically bound together. Theoretical work is needed to confirm whether IRS 13E can be the remnant of a massive cluster. More generally, to address the problem of recent star formation in the vicinity of SgrA* a full census of the hot star population, illustrated in this paper on a small field, remains to be completed. It can be done by deep AO imaging to the condition to acquire data down to 1 μm. Up to now, such data, which appeared essential as shown in the current analysis, have only been possible with NICMOS on HST. Search for optical counterparts of the star-like X-ray sources detected by Chandra in the central parsec is another objective.

Acknowledgements. We gratefully acknowledge helpful discussions with R. Coker which stimulated the close examination of the high-resolution data available on IRS 13. We want to warmly thank Y. Clénet (Meudon Observatory) who made available to us his *L* band AO data. Thanks to the organizing committee led by Tom Geballe, the GC02 Workshop in Kona (Nov. 2002) was an ideal place to improve various issues raised in this paper. Special thanks are also due to T. Ott who sent us the proper motions of the sources of the IRS 13 field, prior to publication.

References

Allen, D. A., & Sanders, R. H. 1986, Nature, 319, 191
Baganoff, F. K., Maeda, Y., Morris, M., et al. 2003, ApJ, 591, 891
Beuzit, J. L., Demailly, L., Gendron, E., et al. 1997, ExA, 7, 285
Blum, R. D., DePoy, D. L., & Sellgren, K. 1995, ApJ, 441, 603
Blum, R. D., Sellgren, K., & DePoy, D. L. 1996, ApJ, 470, 864
Clénet, Y., Rouan, D., Gendron, E., et al. 2001, A&A, 376, 124
Clénet, Y., Lacombe, F., Gendron, E., & Rouan, D. 2003, in Galactic Center Workshop 2002, The Central 300 parsecs (hereafter GC02 Workshop), ed. A. Cotera, S. Markoff, T. R. Geballe, & H. Falcke, Astron. Nachr., 324/S1, 327
Coker, R. F., Pittard, M. J., & Kastner, J. H. 2002, A&A, 383, 568
Diolaiti, E., Bendinelli, O., Bonaccini, D., et al. 2000, A&AS, 147, 335
Eckart, A., Genzel, R., Hofmann, R., Sams, B. J., & Tacconi-Garman, L. E. 1995, ApJ, 445, L23
Eckart, A., Moultaka, J., Viehmann, T., et al. 2003, in GC02 Workshop, Astron. Nachr., 324/S1, 521
Figer, D. F., McLean, I. S., & Najarro, F. 1997, ApJ, 486, 420
Figer, D. F., Kim, S. S., Morris, M., et al. 1999, ApJ, 525, 750
Figer, D. F., Becklin, E. E., McLean, I. S., et al. 2000, ApJ, 533, L49
Genzel, R., Thatte, N., Krabbe, A., Kroker, H., & Tacconi-Garman, L. E. 1996, ApJ, 472, 153
Genzel, R., Eckart, A., Ott, T., & Eisenhauer, F. 1997, MNRAS, 291, 219
Gezari, S., Ghez, A. M., Becklin, E. E., et al. 2002, ApJ, 576, 790
Gerhard, O. 2001, ApJ, 546, L39
Ghez, A. M., Morris, M., & Becklin, E. E. 1999, in The central parsecs of the Galaxy, ed. H. Falcke, A. Cotera, W. J. Duschl, F. Melia, & M. J. Rieke, ASP Conf. Ser., 186, 18
Graves, J. E., Northcott, M. J., Roddier, F. J., Roddier, C. A., & Close, L. M. 1998, SPIE, 3353, 34
Hansen, B. M. S., & Milosavljević, M. 2003, ApJ, 593, L77
Kim, S. S., & Morris, M. 2003, ApJ, 597, 312
Kim, S. S., Figer, D. F., & Morris, M. 2003, in GC02 Workshop, Astron. Nachr., 324/S1, 321
Krabbe, A., Genzel, R., Eckart, A., et al. 1995, ApJ, 447, L95
Lai, O., Véran, J. P., Rigaut, F., et al. 1997, in Optical telescopes of today and tomorrow, ed. A. L. Ardeberg, SPIE, 2871, 859
Libonate, S., Pipher, J. L., Forrest, W. J., & Ashby, M. L. N. 1995, ApJ, 439, 202
Lutz, D., Krabbe, A., & Genzel, R. 1993, ApJ, 418, 244
Magain, P., Courbin, F., & Sohy, S. 1998, ApJ, 494, 472
Maillard, J. P. 2000, in Imaging the Universe in 3 dimensions, ed. E. van Breughel, & J. Bland-Hawthorn, ASP Conf. Ser., 195, 185
Maillard, J. P., Paumard, T., Stolovy, S., & Rigaut, F. 2003, in GC02 Workshop, Astron. Nachr., 324/S1, 263
McMillan, S. L. W., & Portegies Zwart, S. F. 2003, ApJ, 596, 314
Moneti, A., Cernicharo, J., & Pardo, J. R. 2001, ApJ, 549, L203
Morris, M. 1993, ApJ, 408, 496
Morris, M., & Maillard, J. P. 2000, in Imaging the Universe in 3 dimensions, ed. E. van Breughel, & J. Bland-Hawthorn, ASP Conf. Ser., 195, 196
Mengel, S., Eisenhauer, F., Tecza, M., et al. 2000, in Interferometry in Optical Astronomy, ed. P. J. Lena, & A. Quirrenbach, SPIE, 4005, 301
Menten, K. M., Reid, M. J., Eckart, A., & Genzel, R. 1997, ApJ, 475, L111
Muno, M. P., Baganoff, F. K., Bautz, M. W., et al. 2003, ApJ, 589, 225
Najarro, F., Hillier, D. J., Kudritzki, R. P., et al. 1994, A&A, 285, 573
Najarro, F., Krabbe, A., Genzel, R., Lutz, D., & Kudritzki, R. P. 1997, A&A, 325, 700
Ott, T., Eckart, A., & Genzel, R. 1999, ApJ, 523, 248
Ott, T., Genzel, R., Eckart, A., & Schödel, R. 2003, in GC02 Workshop, Astron. Nachr., 324/S1, 543
Ott, T., Schödel, R., Genzel, R., et al. 2003, The Messenger, 111, 1
Paumard, T., Maillard, J. P., Morris, M., & Rigaut, F. 2001, A&A, 366, 466
Paumard, T., Maillard, J. P., & Morris, M. 2003a, in GC02 Workshop, Astron. Nachr., 324/S1, 605 and 2004, A&A, accepted
Paumard, T., Maillard, J. P., & Stolovy, S. 2003b, in GC02 Workshop, Astron. Nachr., 324/S1, 303
Petrov, R. G., Malbet, F., Richichi, A., et al. 2000, in Interferometry in Optical Astronomy, ed. P. J. Lena, & A. Quirrenbach, SPIE, 4006, 68
Portegies Zwart, S. F., & McMillan, S. L. 2002, ApJ, 576, 899
Rieke, G. H., Rieke, M. J., & Paul, A. E. 1989, ApJ, 336, 752
Rieke, M. J. 1999, in The central parsecs of the Galaxy, ed. H. Falcke, A. Cotera, W. J. Duschl, F. Melia, & M. J. Rieke, ASP Conf. Ser., 186, 32
Scoville, N. Z., Stolovy, S. R., Rieke, M., Christopher, M., & Yusef-Zadeh, F. 2003, ApJ, 594, 294
Simon, M., Chen, W. P., Forrest, W. J., et al. 1990, ApJ, 360, 95
Stolovy, S. R., McCarthy, D. W., Melia, F., et al. 1999, in The central parsecs of the Galaxy, ed. H. Falcke, A. Cotera, W. J. Duschl, F. Melia, & M. J. Rieke, ASP Conf. Ser., 186, 39
Tamblyn, P., Rieke, G. H., Close, L. M., et al. 1996, ApJ, 456, 206
Tanner, A., Ghez, A. M., Morris, M., et al. 2002, ApJ, 575, 860
Tanner, A., Ghez, A. M., Morris, M., & Becklin, E. E. 2003, in GC02 Workshop, Astron. Nachr., 324/S1, 597
Wang, Q. D., Gotthelf, E. V., & Lang, C. C. 2002, Nature, 415, 148
Yusef-Zadeh, F., Choote, D., & Cotton, W. 1999, ApJ, 518, L33
Zhao, J. H., & Goss, W. M. 1998, ApJ, 499, L163